Catalysis Today xxx (xxxx) xxx

Contents lists available at ScienceDirect

Catalysis Today

journal homepage: www.elsevier.com/locate/cattod

Non-toxic fluorine-doped TiO_2 nanocrystals from $TiOF_2$ for facet-dependent naproxen degradation

Marta Kowalkińska [a,*], Karol Sikora [b], Marcin Łapiński [c], Jakub Karczewski [c], Anna Zielińska-Jurek [a,*]

[a] Department of Process Engineering and Chemical Technology, Faculty of Chemistry, Gdansk University of Technology, Poland
[b] Department of Inorganic Chemistry, Faculty of Pharmacy, Medical University of Gdansk, Poland
[c] Institute of Nanotechnology and Materials Engineering, Faculty of Applied Physics and Mathematics, Gdansk University of Technology, Poland

ARTICLE INFO

Keywords:
Fluorine-doped TiO_2
Crystal facets engineering
Naproxen degradation
Titanium oxyfluoride
Microtox bioassay

ABSTRACT

In the present study, the photocatalytic degradation of naproxen (NPX), which is a nonsteroidal anti-inflammatory drug (NSAID), frequently detected in drinking water, was investigated. The F-doped TiO_2 with defined morphology was successfully obtained from $TiOF_2$ and applied for photocatalytic degradation under UV–vis and visible light. All samples were characterised by X-ray diffraction, scanning electron microscopy, X-ray photoelectron spectroscopy, zeta potential, diffuse reflectance spectroscopy, and Brunauer–Emmett–Teller surface area analyses. The effect of morphology on the photocatalytic activity of the F-TiO_2 nanostructures with exposed {1 0 1}, {0 0 1} and {1 0 0} facets was studied. Octahedral F-TiO_2 particles with exposed {1 0 1} facets revealed the highest photocatalytic activity, and degraded 100% of the initial NPX concentration after 40 min of the photodegradation process under simulated solar light (UV–vis). Moreover, this sample exhibited the highest TOC removal and NPX degradation under visible light (>420 nm). Based on HPLC-MS analysis, it was assumed that {0 0 1} facets present in fluorinated decahedral nanostructures promote the formation of a dimer, which further hinders the mineralisation rate. Therefore, decahedral nanostructures exposing {1 0 1} and {0 0 1} facets revealed lower photocatalytic activity than octahedral F-TiO_2 particles with exposed {1 0 1} facets, which is also consistent with DFT studies. Finally, toxicity assessment of post-process suspensions using Microtox bioassay confirmed that fluorine-doped octahedral anatase particles are non-toxic, although fluorine ions were the reactants of the synthesis from $TiOF_2$. Overall results showed the possibility of application of highly efficient and environmentally safe fluorine-doped anatase photocatalysts in improved degradation of naproxen.

1. Introduction

An excessive introduction of organic contaminants to water is a serious environmental hazard. The effluents may contain large amounts of toxic organic compounds, which are not susceptible to treatment using conventional methods [1,2]. Therefore, the efficient treatment of wastewaters is an ambitious challenge. Among the group of emerging contaminants, pharmaceuticals and personal care products (PPCP) are extensively and increasingly being detected in the water. PPCPs can be further classified as antibiotics, contrast agents, hormones, and nonsteroidal anti-inflammatory drugs (NSAIDs). Their presence in natural sediments, groundwater, surface water, and even drinking water can hinder the proper functioning of the human body and other organisms in the natural environment. The toxicity and persistence of some pollutants and limited drinking water resources have made it necessary to search for new advanced treatment technologies for environmental protection, applying innovative nanotechnology solutions to purify water from emerging contaminants [3].

Recently, the commonly used worldwide pharmaceuticals from the group of nonsteroidal anti-inflammatory drugs have gained attention due to the concern of possible effects on living aquatic organisms and humans. An example of a pain killer from the NSAIDs group, which occurs in the environment causing an emerging problem, is naproxen (NPX). It is a commonly used drug for treating osteoarthritis in patients, unlike diclofenac and other NSAIDs, because at high doses, it poses a lower vascular risk [4]. Moreover, the prolonged duration of action resulting from a long biological half-life and no need for a prescription are reasons for its popularity in the pharmaceutical market and, as a

* Corresponding authors.
E-mail addresses: marta.kowalkinska@pg.edu.pl (M. Kowalkińska), annjurek@pg.edu.pl (A. Zielińska-Jurek).

https://doi.org/10.1016/j.cattod.2022.11.020
Received 5 August 2022; Received in revised form 28 October 2022; Accepted 14 November 2022
Available online 15 November 2022

consequence, its presence in surface waters. Caban et al. have detected naproxen in ground and surface water in Gdańsk (Poland). In this study, naproxen, next to paracetamol, was one of the most frequently detected active pharmaceutical ingredients in drinking water [5]. Although the established concentration of NPX was at the ng·dm^{-3} level, it is not completely removed during wastewater treatment processes and can bioaccumulate and biomagnify in living organisms, which can cause antibiotic resistance, skin irritation, endocrine disruption or neurotoxic, and even immunotoxic reactions [6,7]. Therefore, the elimination and degradation methods of NPX in WWTP are highly desirable. Among water treatment technologies, heterogeneous photocatalysis is worthy of attention because it allows for the degradation of trace amounts (at the level of a few mg·dm^{-3} to several hundreds of μg·dm^{-3}) of organic pollutants from water or air. If photocatalysts are active under visible light, they open up the possibility of utilising solar irradiation instead of highly energy-consuming UV lamps. However, so far, the low quantum efficiency under visible light and fast charge carriers recombination are still limiting factors in photocatalysis [8].

Titanium (IV) oxide is one of the most promising photocatalysts due to its strong oxidising potential, low cost, and long-term stability against photocorrosion and chemical corrosion [9,10]. However, the large bandgap energy of about 3.2 eV for anatase, and in consequence, the capability of being excited only by ultraviolet light is a limitation for the application of photocatalysis in the presence of solar light. In this regard, attention has been paid to extending the optical response of TiO_2-based photocatalyst. It is of great importance to develop photocatalysts that can be used in both UV and visible light regions. The first attitude is doping by using transition metal cations into TiO_2 lattice. However, this approach often leads to localising d-states deep in the bandgap of titanium (IV) oxide, which acts as the recombination centres for photoexcited electrons and holes and lowers the photocatalytic activity. Moreover, doping may contribute to unfavourably shifting the conduction band below the redox potential of adsorbates, which inactivates the photocatalyst [11]. Therefore, doping with anions, usually non-metal atoms, seems to be a promising alternative for structure modification because they result in the p-states near the valence band, much like other deep donor levels in TiO_2 [12].

Among modified photocatalysts, fluorinated titanium(IV) oxide has been reported as a promising photocatalytic material, including introducing defects to crystal lattice and surface fluorination. The great potential of F-TiO_2 results from strong complexation between F^- and Ti as well as the high electronegativity of fluorine leading to more efficient hole-induced direct water oxidation. Next to changes in surface structure, doping of TiO_2 with fluorine improves its photoreactivity through tailoring the band structure [12]. However, fluorine is toxic to the central nervous system, and excessive exposure to this element can cause harmful effects such as permanent damage to all brain structures, memory dysfunction, and behavioural problems [13]. Moreover, most described fluorinated TiO_2 were synthesised using hydrofluoric acid as a capping agent. The HF-assisted synthesis allows for stabilising high-energetic crystal facets, but their efficiency is low due to the etching of the anatase structure and dissolution–recrystallisation processes [14]. Therefore, titanium oxyfluoride ($TiOF_2$) is a desired precursor because it naturally introduces fluorine ions inside the reaction system. Our previous study showed that the application of $TiOF_2$ enables to control of the growth of selected crystal facets using simple stabilising agents [15].

In this regard, in the present study, faceted F-TiO_2 photocatalysts from the combination of NH_4F and $TiOF_2$ were for the first time successfully synthesised. Furthermore, the photocatalytic activity towards NPX degradation over F-doped titanium(IV) oxide together with the Microtox bioassay test were studied in detail. To our best knowledge, there are no studies of the toxicity assessment of fluorinated TiO_2 with defined morphology. The efficiency of proposed photocatalysts was studied on three parameters: (i) removal of NPX under simulated solar and visible light, (ii) total organic carbon removal, and (iii) toxicity assessment. Finally, the role of surface structure compared with DFT calculations and facets exposition toward NPX degradation pathway were discussed.

2. Experimental

2.1. Synthesis of F-TiO_2

The synthesis of titanium oxyfluoride ($TiOF_2$) by a facile and HF-free solvothermal method was described in our previous study [15]. Titanium (IV) tetrafluoride (TiF_4), 1-butanol, ammonium fluoride (NH_4F), sodium fluoride, and ammonia water (25%) were used as received from Sigma-Aldrich. The synthesis of F-TiO_2 was performed from $TiOF_2$ precursor (0.2 g) dispersed in 50 cm^3 of deionised water. Then, $TiOF_2$ suspension was added to 50 cm^3 of NH_4F solution in NH_4F: $TiOF_2$ molar ratios of 1:1, 2:1, 3:1, 4:1, 5:1 and 10:1. The obtained solution was transferred into a 200 cm^3 Teflon-lined stainless-steel autoclave and kept at 200 °C for 20 h, then cooled down naturally. After each reaction, beige precipitates were centrifuged and washed several times with water and ethanol to remove residual inorganic ions, then dried at 80 °C. The obtained photocatalysts were denoted as A:1, where *A* is the NH_4F: $TiOF_2$ molar ratio used in the synthesis. In addition, the effect of fluorine concentration was studied. In the first series, the appropriate amount of ammonia water was added, preserving the same volume of solution (100 cm^3) as earlier. The second part included the addition of NaF as a source of fluoride ions. In this case, the concentration of F^- was the same as in sample 10:1. Moreover, several attempts were performed with hydrofluoric acid but without success due to etching the anatase structure.

3. Materials characterisation

The characterisation methods applied in this work can be found in the subsection *2.1. Material characterisation* in the Supplementary Information (SI).

4. Results and discussion

The powder X-ray diffraction (XRD) analyses confirmed the phase-pure anatase crystallographic structure of the obtained photocatalysts (see Fig. S1 in Supplementary Information). No signal for any impurities was noticed. However, a close look into the (101) peak might suggest that the lattice is deformed. This peak is slightly shifted, indicating the lattice distortions due to the presence of a dopant. The more NH_4F was used in synthesis, the more remarkable shift was observed. A similar situation occurred when NH_3 or NaF was added during the synthesis. The lattice parameters and unit cell volumes calculated using Rietveld refinement are presented in Table S1.

The obtained photocatalysts' morphologies were examined using scanning electron microscopy. Fig. 1 shows the SEM images of F-TiO_2 prepared from $TiOF_2$. Moreover, SEM observations, including the truncation level and facet identification, are presented in Table S2 in SI. For all samples, the agglomerates composed of smaller nanostructures were observed. However, significant changes in individual photocatalysts can be noted. Firstly, the samples from the series without additives started the agglomeration process in hollow boxes on a bulk microparticle, which originates from the precursor, as well as creating crystal facets. The more NH_4F was used in the synthesis, the more faces from $TiOF_2$ cubes were unfolded, and more nanoparticles were distinguished on microscopy analyses. Therefore, samples n:1 and 4:1 + NaF are decahedral in shape with exposed {0 0 1} and {1 0 1} facets. However, this increased tendency has a limitation. Based on Yang et al., it was assumed that hydrothermal conditions, where water is the solvent, do not allow to stabilise only {0 0 1} facets [16]. Therefore, there is a limitation of synthesis nanostructures with {0 0 1} facets. There is a maximum value of truncation level (also the {0 0 1} to {1 0 1} ratio) and even higher

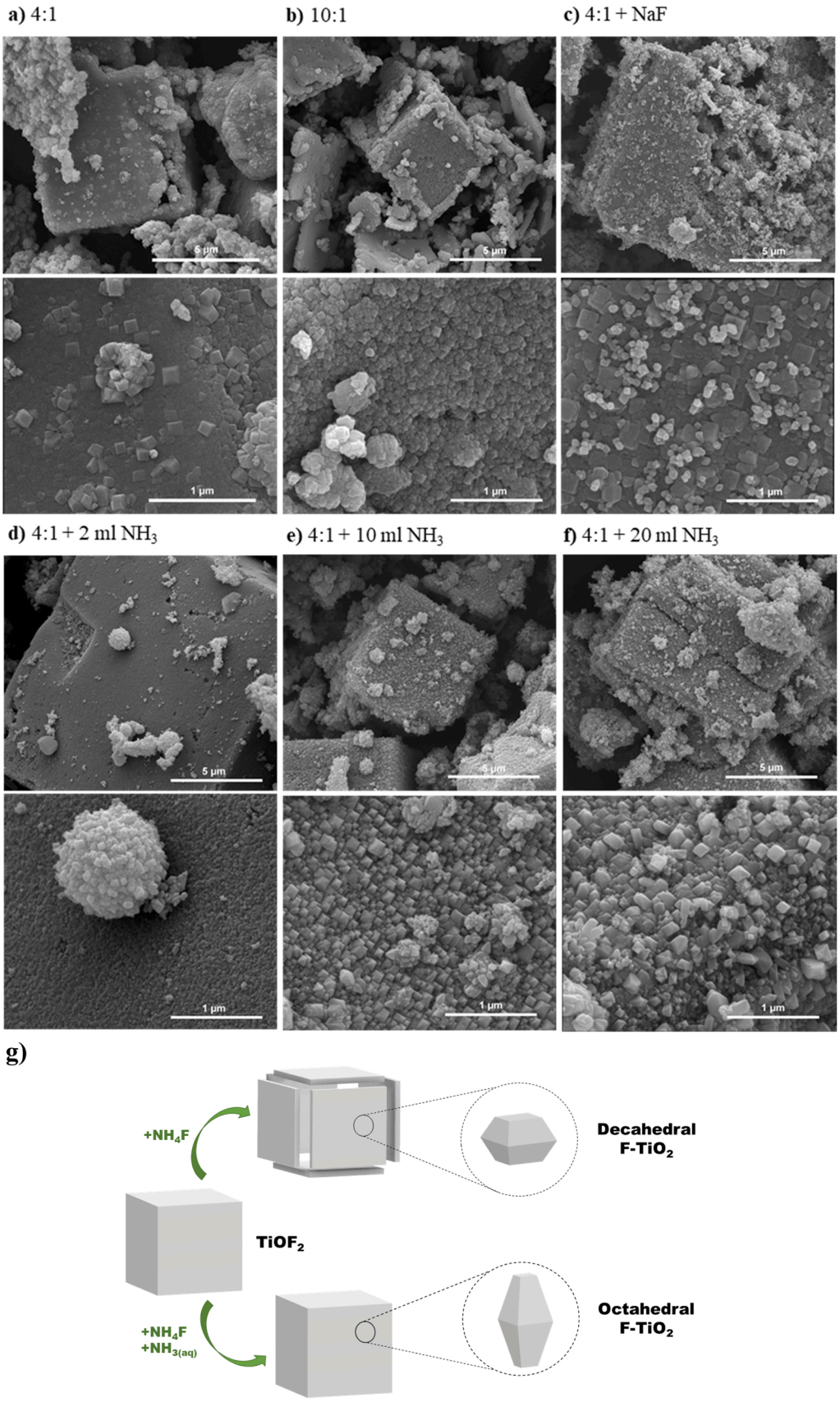

Fig. 1. (a-f) SEM images of F-TiO_2 nanostructures, g) Morphology evolution and transformation of F-TiO_2 from $TiOF_2$.

amount of fluorine in the reaction do not influence on the morphology of the photocatalyst. For further growth of {0 0 1} facets, changing the solvent from water to alcohol is needed [14].

Based on Lee and co-workers' study [17] and the above observations, the mechanism of anatase nanocrystals synthesis from titanium oxyfluoride and ammonium fluoride is proposed and can be described according to the following equations:

$$TiOF_2 + NH_4F \rightarrow NH_4TiOF_3 \quad (1)$$

$$NH_4TiOF_3 + 5H_2O \rightarrow [Ti(OH)_6]^{2-} + 2H^+ + 2HF + NH_4F \quad (2)$$

$$[Ti(OH)_6]^{2-} + 2H^+ \rightarrow TiO_2 + 4H_2O \quad (3)$$

According to Eqs. (1)–(3), three important roles of ammonium fluorine can be highlighted: i) a source of the intermediate product of NH_4TiOF_3, which can further hydrolyse to TiO_2, ii) capping agent, and iii) fluorine ions as the self-etching agent instantaneously produced in the system. However, the addition of $NH_{3(aq)}$ to the reaction system preserved the bulk cube originating from titanium oxyfluoride and prevented hollowing microparticles out. Ammonia molecules act as F^- scavengers, preventing adsorption on the photocatalyst's surface. Fluorine ions stabilise the {0 0 1} facet [18], which explains that on the cubes' faces, small nanoparticles with octahedral shapes with {1 0 1} facets are noted, as presented in Fig. 1d-e. For octahedral nanostructures, adding more ammonia to the synthesis caused lowering the truncation level and more distinct {1 0 1} facet exposition. So far, the synthesis of octahedral TiO_2 requires specific capping agents like a combination of hydrazine and sulphate ions [19] or using $Na_2Ti_3O_7$ phase [20]. The advantage of using $TiOF_2$ as a precursor is the simplification of the procedure of octahedral titanium (IV) oxide synthesis with good reproducibility. However, as presented in Fig. 1f, adding a high amount of $NH_{3(aq)}$ to the reaction system caused the formation of {1 0 0} facets, which was consistent with our previous study [15].

To confirm the presence of fluorine in the photocatalyst's structure, Energy Dispersive X-Ray Analysis (EDX) was performed for selected samples (Table S2 in Supplementary Information). The presence of fluorine was confirmed in most of the analysed samples. In the case of series + NH_3, the fluorine content is lower due to decreased amount of surface fluorine, replaced by -OH groups.

Based on SEM and EDX analysis, the schematic synthesis procedure of the fluorinated TiO_2 with defined morphology is presented in Fig. 1g. Overall, adding ammonium fluorine without additives enables to grow

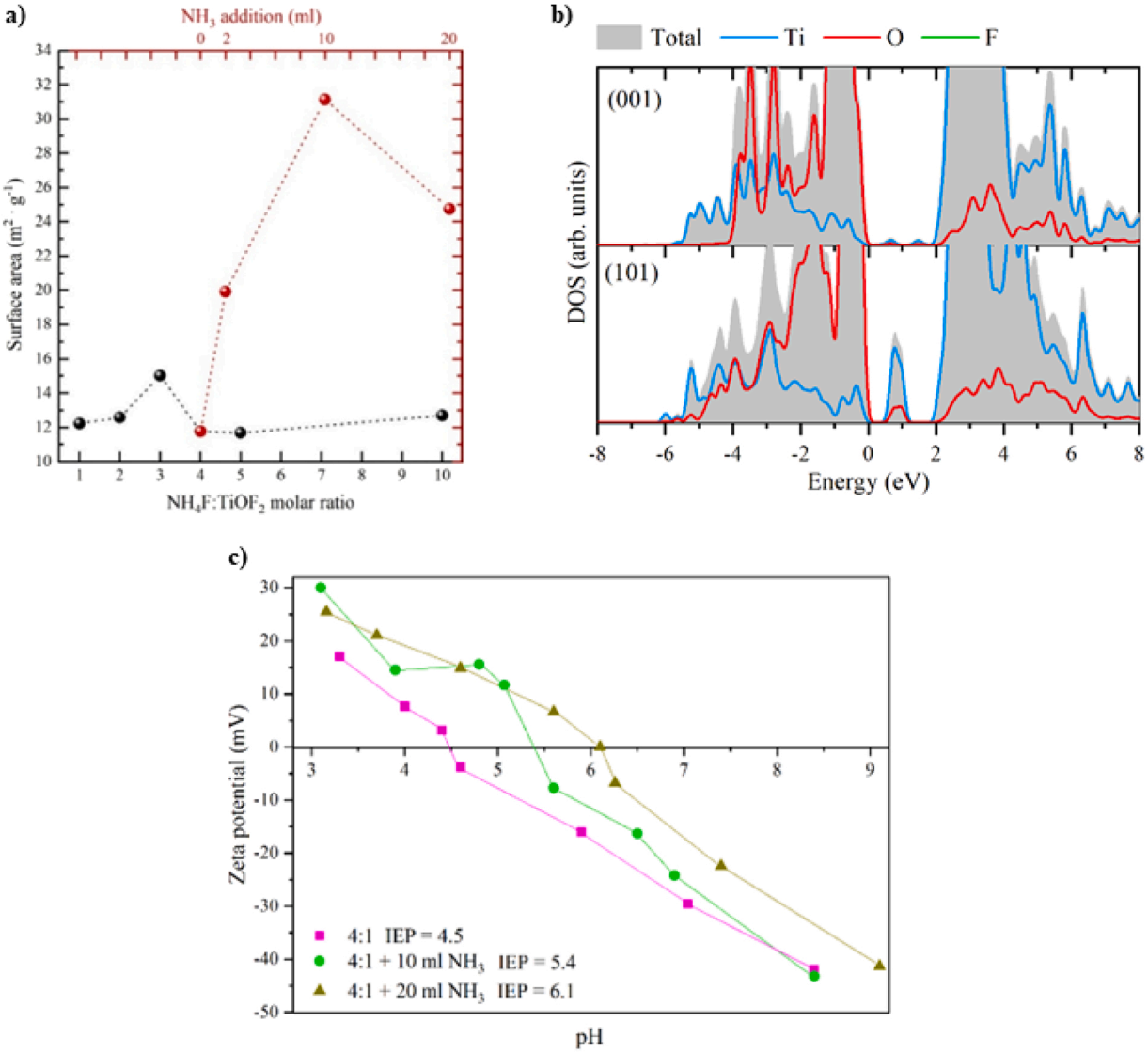

Fig. 2. a) A relationship between the surface area of photocatalysts and NH_4F: $TiOF_2$ ratio (black axis) or NH_3 volume used during synthesis (the dark red one), b) The total and partial density of states for F-doped (101), and (001) slab model, obtained with the GGAU methodology, c) Zeta potential determined from the electrophoretic mobility in dependence of the pH, $I = 1 \cdot 10^{-2}$ M KCl.

decahedral nanoparticles with exposed {1 0 1} and {0 0 1} facets. If a certain amount of ammonia water is introduced to the reaction system, only {1 0 1} facets are present in octahedral nanostructures. Furthermore, the XPS analysis showed that the surface of the series with $NH_{3(aq)}$ addition did not contain fluoride (see Fig. S2 in Supplementary Information). The most photocatalytic active sample of octahedral F-TiO_2 had negligible F^- ions on the surface. However, the fluorine atoms are present in the lattice, which was confirmed by EDX analysis. For sample with NaF presence, the content of F^- was about 7%, and it was slightly lower than for F-TiO_2 without additives.

Among the F-TiO_2 samples, the relatively highest surface area in the series is noticed for NH_4F: $TiOF_2$ with a 3:1 molar ratio, see in Fig. 2a. However, the addition of NH_3 to the reaction system contributed to the growth of {1 0 1} facets and increased the surface area of photocatalysts. However, an increase in S_{BET} value is limited, and the decrease of the surface area for the 4:1 + 20 cm^3 NH_3 sample is noted, which may be a result of nanocrystals formation with {1 0 0} facets.

To better understand the optical properties of F-TiO_2 nanostructures, DR/UV–vis spectra were analysed (Fig. S3 in SI) and compared with theoretical calculations using the Density Functional Theory (DFT) method. The DOS simulation is depicted in Fig. S4 in SI. The total and partial density of states for F-doped (101) and (0 0 1) slab model is presented in Fig. 2b. The bandgap of (0 0 1) and (1 0 1) F-doped surface were 1.84 eV and 1.64 eV, respectively. Therefore, the {1 0 1} facets in fluorine-doped anatase nanostructures are supposed to reveal better visible light response than {0 0 1} facets. Similar to bulk F-doped anatase, all models are characterised by the presence of midgap states. However, the significant difference between these two slabs is in the type of midgap states. A distinct DOS band in the (1 0 1) surface slab can be noted, opposite the small two bands in (0 0 1). This change in electronic structure is a reason for enhanced light absorption in the visible region. Therefore, the decahedral F-TiO_2 photocatalysts as a combination of {1 0 1} and {0 0 1} facets may exhibit lower photocatalytic activity under visible light compared to octahedral F-TiO_2 with exposed only {1 0 1} facets.

Furthermore, to study the surface properties of the F-TiO_2 photocatalysts, the electrophoretic mobility of these particles at different pH values (zeta potential) was investigated. The isoelectric point (IEP), which represents the pH where the electrophoretic mobility changes from positive to negative was determined for sample 4:1 of F-TiO_2 exposing {1 0 1} and {0 0 1} facets, sample 4:1 + 10 ml NH_3 of F-TiO_2 exposing {1 0 1} facets, and sample 4:1 + 20 ml NH_3 with exposed {1 0 1} and {1 0 0} facets (see Fig. 2c). In the case of 4:1 + 20 ml NH_3 with exposed {1 0 0} facets, the IEP = 6.1 is close to the values reported in the literature for anatase [21]. However, the shift towards acidic conditions was observed and the IEP for octahedral and decahedral F-TiO_2 were 5.4 and 4.5, respectively. So, the following order of IEP based on the facet exposition can be noticed: {0 0 1} < {1 0 1} < {1 0 0}. These results can be explained by differences in the surface atom rearrangement and electronic distribution on the surface. In consequence, there will be a different rate of surface hydroxylation and protonation for particular facets. The {0 0 1} facets, due to F^- stabilisation, are the most negatively charged in comparison with {1 0 1} and {1 0 0} facets, which is consistent with the existing literature [22]. The higher stability of suspension was noticed at a pH of about 4 and above 7. In addition, these results were compared with the initial pH of the photocatalyst suspension in NPX solution. The pH of the photocatalyst suspension was 4.8 for octahedral F-TiO_2 (sample 4:1 + 10 ml NH_3) and 4.3 for decahedral F-TiO_2 (sample 4:1), whereas pure NPX solution had the initial pH of 4.9. The pKa of NPX is about 4.2, so during photocatalysis with F-TiO_2, naproxen occurs in a deprotonated form with a negative charge. During NPX removal, the photocatalyst surface was positively charged (pH < pH_{IEP}), which facilitated the attraction of the deprotonated form of the naproxen molecule at the photocatalyst surface.

The photocatalytic activity of the as-prepared F-doped TiO_2 was investigated in the reaction of NPX degradation under UV–vis and visible (λ > 420 nm) light. The results are presented in Fig. 3. Firstly, the photolysis of NPX was analysed to notice the differences between processes with or without photocatalyst. The concentration of NPX decreased rapidly during photolysis under UV–vis light (Fig. 3a and c), and after 90 min of irradiation, the observed reduction of naproxen concentration was 91%. The high level of photolytic processes can be explained by deprotonation of carboxylic acid group in NPX molecule, which occurred, when pH > pKa. This deprotonated NPX molecule, having a $\pi \rightarrow \pi^*$ conjugation system, is supposed to easily undergo photolysis. Marotta et al. reported the photolysis of naproxen under monochromatic irradiation with a wavelength of 254 nm (UVC light), indicating a significant role of dissolved oxygen in a solution due to its predominant role in the generation of singlet oxygen at aerated conditions. The major by-product was 1-(6-methoxy-2-naphthyl)ethanol, which molecule differs from NPX compound replacement of -COOH group by -OH [23]. The photolysis of NPX in visible light was significantly lower than NPX removal under UV–vis light. The photocatalytic degradation process was more effective than the photolysis. All F-TiO_2 photocatalysts were highly photoactive in NPX decomposition. What is worth noticing, the removal rate was dependent on the morphology of the F-doped TiO_2 photocatalyst. In the case of samples 5:1 and 10:1, about 100% of NPX was degraded after 60 min of irradiation. Among the nanostructures with exposed {1 0 1} and {0 0 1} facets, samples with a higher molar ratio of NH_4F to $TiOF_2$ were the most active in the series without additives (NaF or NH_3). Furthermore, the presence of sodium fluoride in the synthesis (sample 4:1 + NaF) of decahedral fluorinated anatase particles negatively affected NPX degradation (see Fig. 3c). However, for octahedral F-TiO_2 with exposed {1 0 1} facets (sample 4:1 + 10 cm^3 NH_3), the degradation rate markedly increased, and after 40 min, naproxen was completely degraded.

Based on NPX degradation analyses performed in the presence of scavengers, it can be noticed that •OH are the predominant reactive oxygen species in NPX degradation using octahedral F-TiO_2, whereas $O_2^{\bullet -}$ are more important in the photodegradation in the presence of decahedral F-TiO_2 (see Fig. S5 in SI). Finally, the relative photonic efficiency was calculated and the value reached 2.94 for NPX solution. Detailed information about these calculations are in Supporting Information.

Regarding the photocatalytic activity under vis light, the higher NH_4F: $TiOF_2$ ratio resulted in increased and more efficient NPX photodegradation in the presence of the obtained F-doped decahedral anatase particles (see Fig. 3b and d). Furthermore, the series with F-doped octahedral anatase particles (samples 4:1 + NH_3) revealed much more efficient naproxen photodegradation than decahedral F-TiO_2 under vis light. The highest visible-light driven photocatalytic activity was observed for sample 4:1 + 10 ml NH_3. After 120 min, 63% of naproxen was degraded. The significant difference is noticed while comparing samples 10:1 and 4:1 +NaF, which have the same fluorine amount in the reaction system. For sample 10:1, 48% of NPX removal was observed after 120 min of visible light irradiation, whereas the sample 4:1 + NaF reached only 31% in the same process parameters. The results for this sample can be explained by the presence of Ti^{3+} on the 4:1 + NaF surface, which may act as recombination centres and, in consequence, decrease the photocatalytic activity. The calculated constant rates based on a pseudo-first order model are presented in Table S3 in Supplementary Information. The visible light-driven photocatalysts towards NPX degradation were reported previously, such as AgBr-α-$NiMoO_4$ [24], reduced graphene oxide/$ZnIn_2S_4$ [25], Ag/AgI/ZnO [26] or TiO_2 immobilised on polyacrylonitrile/multiwall carbon nanotubes composite (PAN-CNT/TiO_2-NH_2) [27]. These materials rapidly degraded NPX under visible light irradiation, although the light intensity used during the photocatalytic experiment was high (~100 mW/cm^2). Herein, we have focused on single-component photocatalyst with simple synthesis conditions and unsophisticated modifications. Our results showed that using photocatalysts for efficient naproxen removal without high-energy rays is possible.

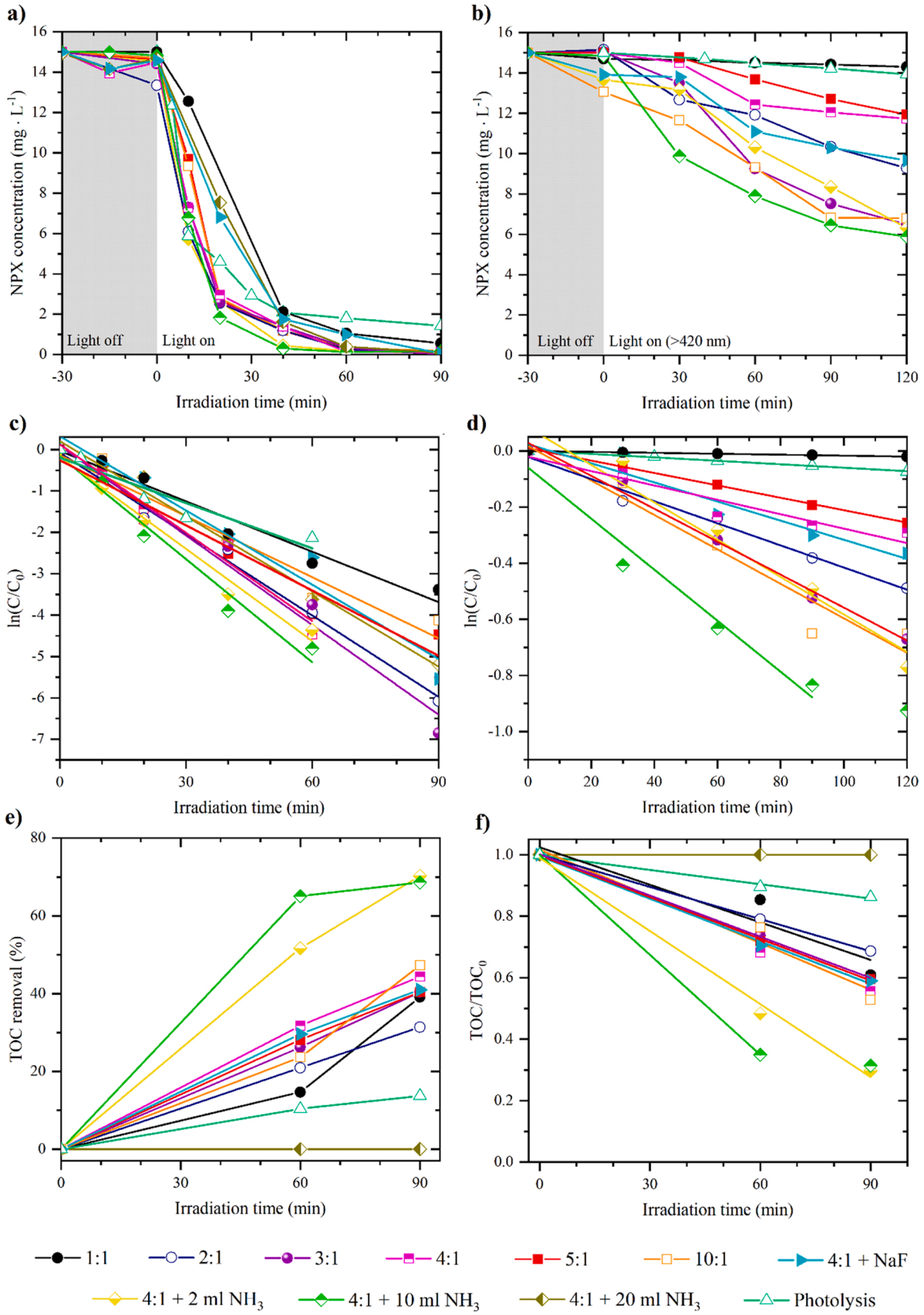

Fig. 3. Photocatalytic degradation of naproxen as a function of concentration (a, b) and ln(C/C$_0$) (c, d); photocatalytic performance was determined under UV–vis irradiation (a, c) and visible (> 420 nm) light (b, d); TOC removal in the presence of F-TiO$_2$ photocatalysts after photocatalytic process (e, f).

The TOC removal in the presence of F-TiO_2 photocatalysts after 60 and 90 min of UV–vis irradiation is presented in Fig. 3e. During photolysis, NPX molecules undergo partial mineralisation, but this reaction's mineralisation rate is slow. For the photocatalytic process, the efficiency of TOC reduction increased for all F-TiO_2 materials except the sample 4:1 + 20 cm^3 NH_3, probably due to the presence of {1 0 0} facets. These observations are consistent with Xu et al., who have suggested that {1 0 0} facets are strongly reductive, and electrons transferred to the surface can reduce H^+ into H_2 effectively [28]. For NH_4F+$TiOF_2$ series with decahedral nanostructures, all photocatalysts exhibit a similar TOC removal in the range of 30–50% after 90 min of the photocatalytic process. Similar results were obtained for the sample 4:1 + NaF, so the type of fluorine source does not influence the NPX conversion to CO_2. Meanwhile, a significant enhancement in TOC removal of about 70% was observed for series with ammonia water addition. The most efficient photocatalyst was the sample 4:1 + 10 cm^3 NH_3, for which 65% of TOC reduction was noticed after 60 min of the photocatalytic process. This sample also revealed the highest photocatalytic activity under UV–vis and vis light irradiation. Such high TOC removal rates have so far been observed for commercial P25 [29,30] or ternary photocatalysts like single atom-dispersed silver and carbon quantum dots co-loaded with carbon nitride [31]. However, the addition of a higher amount of $NH_{3(aq)}$ contributed to growing {1 0 0} facets, which in consequence, probably inhibited the degradation process and mineralisation. These results are in agreement with our previous study regarding facet-dependent photocatalytic activity towards phenol degradation using TiO_2 with defined morphology. The octahedral nanostructures with exposed {1 0 1} facets are more suitable for phenol mineralisation than decahedral ones due to the increased formation of $O_2^{\bullet-}$ on the {1 0 1} surface and favoured electron localisation on the surface [15]. In this study, octahedral F-TiO_2 is more efficient in NPX mineralisation than decahedral nanostructures, suggesting that the NPX degradation pathway can be facet-dependent.

For a better understanding of the NPX degradation pathway, post-process water after 10 and 20 min of photocatalysis and 90 min of photolysis were analysed using liquid chromatography-mass spectrometry (HPLC/MS). Table S4 shows the detected intermediate products, and Fig. 4a depicts the detected products of NPX photocatalytic degradation. In the case of photolysis, the presence of two principal pseudo-molecular ions representing - 2-acetyl-6-methoxynaphthalene (NPX 1) and dimer $C_{26}H_{26}O_4$ can be observed. It can be assumed that the dimerisation process leads to the creation of more complex compounds which are supposed to be less susceptible to photo-induced degradation processes. Therefore, the TOC removal will be lower when the dimer is formed. However, partial mineralisation during the photolytic process is observed, which is probably a result of partial naproxen decarboxylation [32,33]. Next to NPX 1, 1-(6-methoxy-2-naphthyl)ethanol (NPX 2) and 2-ethyl-6-methoxynaphtalene were noticed. Surprisingly, in the case of

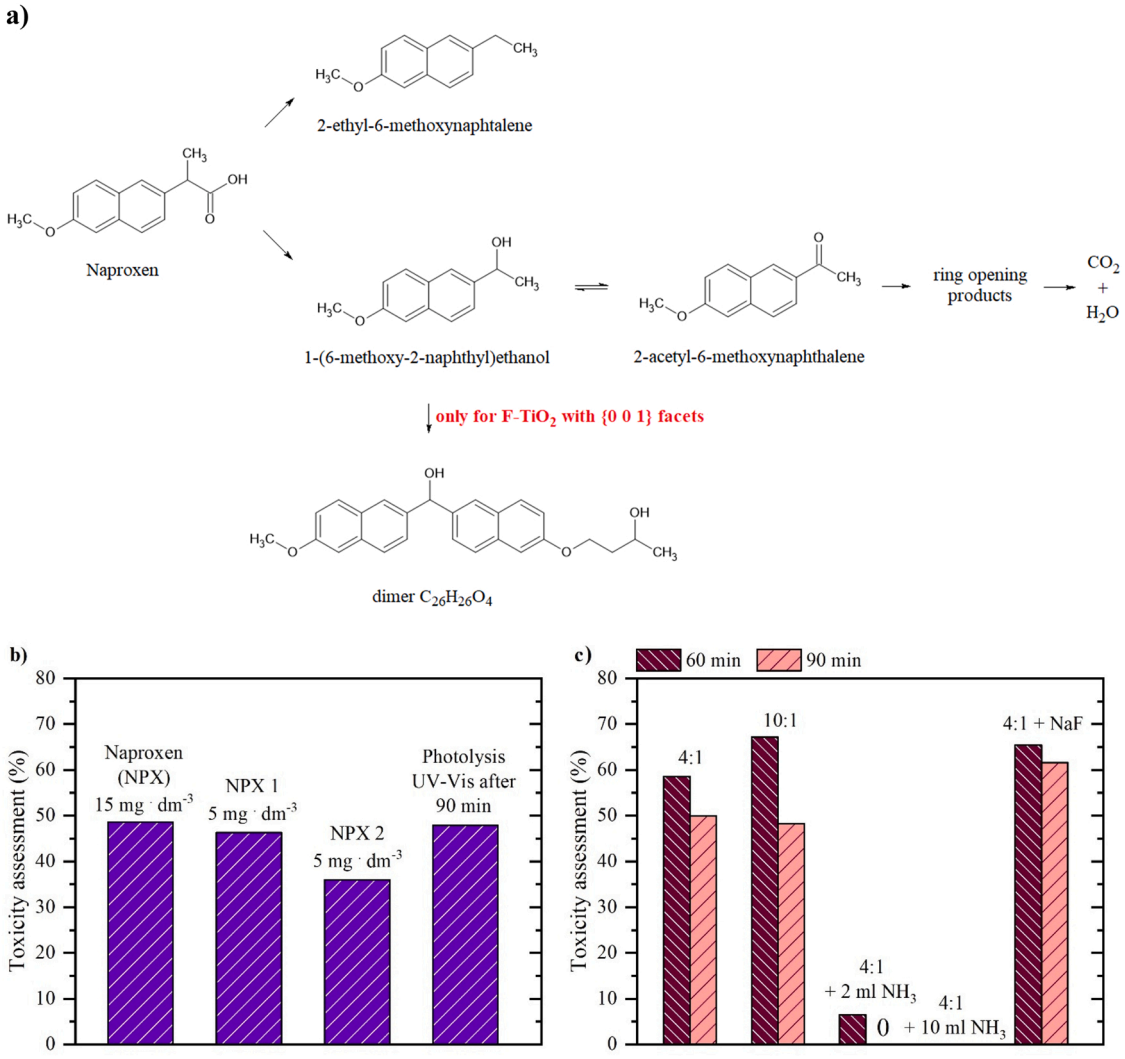

Fig. 4. a) Products of NPX photocatalytic degradation under UV–vis irradiation, Microtox test of b) NPX and derivatives solutions and c) post-treatment wastewater using selected photocatalysts.

octahedral F-TiO_2 with {1 0 1} facets, no products of dimerisation were detected, in opposite to decahedral particles. These results indicate different NPX degradation pathways depending on facet exposition. When {0 0 1} facets are exposed in the photocatalyst, the formation of dimer $C_{26}H_{26}O_4$ is induced, in opposite to {1 0 1} facets. By analogy to photolysis, the dimerisation process is unfavourable for NPX removal because it inhibits the mineralisation to CO_2 and H_2O. Therefore, the highest TOC removal was noticed for the photocatalyst 4:1 + 10 cm^3 NH_3, which is octahedral in shape, and dimer compounds were not produced during the degradation process. More detailed studies about by-products formation are presented in Fig. S7 in Supporting Information.

To study the toxicity of NPX mixture in the presence of F-TiO_2 photocatalysts, Microtox bioassays were performed. The results are presented in Fig. 4. Firstly, the NPX initial solution and two by-products were analysed. It can be observed that the toxicity of NPX is moderate (49%). The presented results of the NPX solution are comparable with the literature [29]. However, there is a lack of information about the toxicity of main by-products. In this regard, additional measurements were performed in the maximum concentration detected by HPLC analysis. Remarkably, 2-acetyl-6-methoxynaphthalene (NPX 1) is similarly toxic to naproxen, although the concentration of this intermediate is just 5 mg · dm^{-3}. This effect may be a result of changes in the aliphatic chain (-CH(CH_3)-COOH for NPX and -C(O)-CH_3 for NPX 1). The toxicity assessment for 1-(6-methoxy-2-naphthyl)ethanol (NPX 2) showed lower inhibition of *Vibrio fisheri* bioluminescence than two previous compounds, which may be a result of replacing the ketone group with the hydroxyl group.

What is worth noticing the direct NPX removal during the photolysis process did not decrease the toxicity (see Fig. 4c). In the case of photocatalysis using F-doped TiO_2, the rise in toxicity after 60 min of the photocatalytic degradation process is observed for 4:1 and 10:1 samples. Two reasons for this effect can be indicated. Firstly, F-TiO_2 decahedral nanostructures had fluorine ions on the surface, necessary to create {0 0 1} facets, which are supposed to be toxic. Secondly, {0 0 1} facets promote the formation of a dimer, which may be more toxic than other compounds presented in Figure 5a. Remarkably, no inhibition of bacterias' bioluminescence is observed in the presence of octahedral F-TiO_2 in NPX solution, which also correlates well with the high TOC removal of this sample. This photocatalyst also had negligible F^- ions on the surface, confirmed by the XPS analysis. Therefore, the application of F-TiO_2 with exposed {1 0 1} facets is supposed to be environmentally friendly. On the other hand, the post-treatment wastewater after the photocatalytic process in the presence of sample 4:1 + NaF is the most toxic in the series. By analogy to HPLC analysis, these nanostructures promote different degradation pathways without NPX 1 formation; therefore, these by-products may be more toxic than from other series.

5. Conclusions

Fluorine-doped anatase nanostructures synthesised from titanium oxyfluoride with defined morphology were for the first time obtained and applied for efficient naproxen photocatalytic degradation under UV–vis and vis light. The effect of NH_3, NaF and NH_4F introduced during solvothermal synthesis on preparation of F-TiO_2 nanocrystals with exposed {0 0 1}, {1 0 1} and {1 0 0} facets was investigated. The octahedral F-TiO_2 with exposed {1 0 1} facets and fluorine-free surface exhibited the highest photocatalytic activity. Moreover, this sample (4:1 + 10 cm^3 NH_3) revealed the highest efficiency of NPX removal under visible light (> 420 nm) and the highest TOC removal under simulated solar light. The high photocatalytic activity can be explained by DFT calculations, which suggest the presence of additional surface states when fluorine atoms are introduced to the (1 0 1) surface as well as a lower surface bandgap than (0 0 1). The facet dependence was crucial in changes in the concentration of 2-acetyl-6-methoxynaphthalene. Remarkably, our study showed that {0 0 1} facets of F-doped decahedral anatase particles promote the dimerisation process, inhibiting efficient NPX removal. Finally, Microtox bioassay tests confirmed that the application of octahedral fluorine-doped anatase particles is safe for the environment. In view of the excellent photocatalytic performance and non-toxicity, the fluorinated TiO_2 nanomaterial has the potential for practical application, thus providing a new idea for wastewater treatment from active pharmaceutical ingredients.

CRediT authorship contribution statement

Marta Kowalkińska: Conceptualization, Investigation, Formal analysis, Writing – original draft, Writing – review & editing. **Karol Sikora:** Investigation, Formal analysis. **Marcin Łapiński:** Investigation, Formal analysis. **Jakub Karczewski:** Investigation. **Anna Zielińska-Jurek:** Conceptualization, Methodology, Validation, Supervision, Writing – review & editing, Project administration, Funding acquisition.

Declaration of Competing Interest

The authors declare the following financial interests/personal relationships which may be considered as potential competing interests: Anna Zielińska-Jurek reports financial support was provided by National Science Centre Poland.

Data availability

Data will be made available on request.

Acknowledgements

The research was financially supported by the Polish National Science Centre, Grant No. 2018/30/E/ST5/00845.

Appendix A. Supplementary material

Supplementary data associated with this article can be found in the online version at doi:10.1016/j.cattod.2022.11.020.

References

[1] M. Pirilä, M. Saouabe, S. Ojala, B. Rathnayake, F. Drault, A. Valtanen, M. Huuhtanen, R. Brahmi, R.L. Keiski, Top. Catal. 58 (2015) 1085–1099.
[2] S.N. Ahmed, W. Haider, Nanotechnology 29 (2018), 342001.
[3] O. Fawzi Suleiman Khasawneh, P. Palaniandy, Civ. Environ. Eng. Rep. 29 (2019) 1–33.
[4] D.J. Angiolillo, S.M. Weisman, Am. J. Cardiovasc. Drugs 17 (2017) 97–107.
[5] M. Caban, E. Lis, J. Kumirska, P. Stepnowski, Sci. Total Environ. 538 (2015) 402–411.
[6] D. Wojcieszyńska, U. Guzik, Appl. Microbiol. Biotechnol. 104 (2020) 1849–1857.
[7] L. Corominas, P. Gimeno, C. Constantino, P. Daldorph, J. Comas, J. Hazard. Mater. 407 (2021).
[8] S.K. Loeb, P.J.J. Alvarez, J.A. Brame, E.L. Cates, W. Choi, J. Crittenden, D. D. Dionysiou, Q. Li, G. Li-Puma, X. Quan, D.L. Sedlak, T. David Waite, P. Westerhoff, J.H. Kim, Environ. Sci. Technol. 53 (2019) 2937–2947.
[9] G. Nabi, W. Raza, M.B. Tahir, J. Inorg. Organomet. Polym. Mater. 30 (2019) 1425–1429.
[10] M. Saif, S.M.K. Aboul-Fotouh, S.A. El-Molla, M.M. Ibrahim, L.F.M. Ismail, J. Nanopart. Res. 14 (2012).
[11] W. Choi, A. Termin, M.R. Hoffmann, J. Phys. Chem. 98 (1994) 13669–13679.
[12] J. Wang, D.N. Tafen, J.P. Lewis, Z. Hong, A. Manivannan, M. Zhi, M. Li, N. Wu, J. Am, Chem. Soc. 131 (2009) 12290–12297.
[13] K. Dec, A. Łukomska, D. Maciejewska, K. Jakubczyk, I. Baranowska-Bosiacka, D. Chlubek, A. Wąsik, I. Gutowska, Biol. Trace Elem. Res. 177 (2017) 224–234.
[14] S. Dudziak, M. Kowalkińska, J. Karczewski, M. Pisarek, K. Siuzdak, A. Kubiak, K. Siwińska-Ciesielczyk, A. Zielińska-Jurek, Appl. Surf. Sci. 563 (2021), 150360.
[15] M. Kowalkińska, S. Dudziak, J. Karczewski, J. Ryl, G. Trykowski, A. Zielińska-Jurek, Chem. Eng. J. 404 (2021), 126493.
[16] H.G. Yang, G. Liu, S.Z. Qiao, C.H. Sun, Y.G. Jin, S.C. Smith, J. Zou, H.M. Cheng, G. Q. Lu, J. Am. Chem. Soc. 131 (2009) 4078–4083.
[17] H.K. Lee, S.W. Lee, Chem. Lett. 44 (2015) 604–606.
[18] T.R. Gordon, M. Cargnello, T. Paik, F. Mangolini, R.T. Weber, P. Fornasiero, C. B. Murray, J. Am. Chem. Soc. 134 (2012) 6751–6761.
[19] L. Gai, Q. Mei, X. Qin, W. Li, H. Jiang, X. Duan, Mater. Res. Bull. 48 (2013) 4469–4475.

[20] P. Mikrut, M. Kobielusz, W. Macyk, Electrochim. Acta 310 (2019) 256–265.
[21] K. Kobayashi, M. Takashima, M. Takase, B. Ohtani, Catalysts 8 (2018).
[22] H. Park, W. Choi, J. Phys. Chem. B 108 (2004) 4086–4093.
[23] R. Marotta, D. Spasiano, I. Di Somma, R. Andreozzi, Water Res. 47 (2013) 373–383.
[24] S.K. Ray, D. Dhakal, S.W. Lee, Chem. Eng. J. 347 (2018) 836–848.
[25] K. Fun, Y. Pan, C. Ding, J. Shi, H. Deng, Catalysts 10 (2020).
[26] C. Ding, K. Fu, M. Wu, S. Gong, J. Liu, J. Shi, H. Deng, J. Photochem. Photobiol. A Chem. 414 (2021), 113283.
[27] A. Uheida, A. Mohamed, M. Belaqziz, W.S. Nasser, Sep Purif. Technol. 212 (2019) 110–118.
[28] H. Xu, S. Ouyang, P. Li, T. Kako, J. Ye, ACS Appl. Mater. Interfaces 5 (2013) 8262.
[29] D. Kanakaraju, C.A. Motti, B.D. Glass, M. Oelgemöller, Chemosphere 139 (2015) 579–588.
[30] A. Romeiro, M.E. Azenha, M. Canle, V.H.N. Rodrigues, J.P. Da Silva, H.D. Burrows, ChemistrySelect 3 (2018) 10915–10924.
[31] F. Wang, Y. Wang, Y. Feng, Y. Zeng, Z. Xie, Q. Zhang, Y. Su, P. Chen, Y. Liu, K. Yao, W. Lv, G. Liu, Appl. Catal. B 221 (2018) 510–520.
[32] G. Fan, J. Zhan, J. Luo, J. Zhang, Z. Chen, Y. You, Catal. Sci. Technol. 9 (2019) 4614–4628.
[33] F. Méndez-Arriaga, J. Gimenez, S. Esplugas, J. Adv. Oxid. Technol. 11 (2008) 435–444.